Developing a facile g-C3N4 coated stainless steel mesh with different superhydrophilic/underwater superoleophobic and superoleophilic behavior for oil-water separation

Sonia Mir
Amirkabir University of Technology
Abbas Naderifar
Amirkabir University of Technology
Alimorad Rashidi (rashidiam@ripi.ir)
Research Institute of Petroleum Industry https://orcid.org/0000-0001-6753-1939
Mahshad Alaei
Research Institute of Petroleum Industry

Research Article

Keywords: wettability behavior of g-C3N4 nanosheets, oil-water separation, superhydrophilic/underwater oleophobic surfaces, superoleophilic surfaces

Posted Date: February 4th, 2022

DOI: https://doi.org/10.21203/rs.3.rs-1252680/v1

Abstract

There is an increasing demand for the development of inexpensive and effective approaches for the oil–water separation due to the global concern in oil industries. The present study was conducted to fabricate graphitic carbon nitride/thermoplastic polyurethane (g-C_3N_4/TPU) coated stainless steel meshes via the dip-coating method to investigate the capability of g-C_3N_4 nanosheets (CN-NS) in oil-water separation. CN-NS was synthesized using the polycondensation process followed by exfoliation with Hummer's method. We studied the effect of TPU and CN-NS concentration on wettability behavior to obtain an optimized coating solution. CN-NS coated mesh showed superoleophilic/hydrophobic behavior at CN-NS:TPU ratio of 50:50 and it efficiently passed oil from the emulsified water-in-oil mixture (with 50%wt. oil) with the efficiency of 99%. The wettability behavior of superhydrophilic/underwater superoleophobic was also obtained at CN-NS:TPU ratio of 80:20 and it was able to separate water from the emulsified water-in-oil mixture with the efficiency of 79% under gravity. Both filters were able to separate free water and oil mixtures with flux and efficiency of 6114 $L.m^{-2}.h^{-1}$ and ~99.99%, respectively. The mechanism of wettability behavior of the coating is mainly related to the functional groups on the edge of g-C_3N_4-NS, thus increasing the hydrophilic properties of the surface. In addition, the micro-nano hierarchical structure of the surface coating improves its roughness due to the presence of CN-NS, which is effectively embedded into the hydrophilic TPU. More importantly, commercially available TPU chemical and simple fabrication of g-C_3N_4 from an inexpensive precursor, make the method reported herein as a significant alternative for large-scale application.

Introduction

Oil and water separation has become a worldwide subject with growing challenges of the production of water in oil emulsions. The presence of water in oil causes problems, such as corrosion and catalyst deactivation, in downstream processes. Therefore, it is necessary to develop an effective method for oil-water separation. Recently, filtration media such as metal meshes, polymer membranes and cotton fabrics based on superoleophilic and superhydrophilic/underwater superoleophobic materials have been applied for highly efficient separation of water-in-oil (W/O) or oil-in-water (O/W) mixtures, respectively (Wang, Wang et al. 2018, Zhang, Wang et al. 2019, Lin, Salem et al. 2020, Sun, Zhang et al. 2020).

Various physical and chemical methods of surface modification have been used to render filtration media with specific wetting properties. The prepared filtration media with appropriate pore size and engineering morphologies are capable to separate oil-water emulsions (Zhu, Dudchenko et al. 2017, Su, Liu et al. 2018). Inorganic materials as promising candidate coating materials with appropriate mechanical and thermal properties are utilized in coating materials. Stainless steel mesh (SSM) coated with many nanoparticles such as: silica nanoparticles (Yang, Pi et al. 2010), TiO_2 (Yu, Chen et al. 2014, Agano, Villanueva et al. 2021), ZnO nanowires (Tian, Zhang et al. 2011, Tian, Zhang et al. 2012), Cu micro-flakes (Song, Huang et al. 2014) and so on have been reported for oil/water and water/oil separation. However,

these developed surface coatings are often operationally and chemically intensive and require expensive material or complex precursor fabrication processes.

Although many nanoparticles have been reported for water and oil separation in various studies, carbon nitride nanoparticles have rarely been used for oil-water separation. Simple fabrication process of carbon nitrides, low cost and high commercial availability of their raw materials, give them an advantage over other nanoparticles to be used in the preparation of filters for oil-water separation in industry.

Graphitic carbon nitride (g-C_3N_4) has received tremendous attention as a novel carbon-nitride nanomaterial because of its special physicochemical characteristics, eco-friendly nature, suitable band gap, special electronic band structure and easy functionalization (Du, Zou et al. 2015, Ong, Tan et al. 2016). Other notable potentials of this material include its easy preparation from cheap and available precursors of urea (Liu, Li et al. 2015) or melamine(Fang, Fan et al. 2015, Li, Lian et al. 2016). g-C_3N_4 has a layered structure with weak intermolecular van der Waals forces or electrostatic forces (Niu, Zhang et al. 2012, Xie, Zhang et al. 2013). The structure of g-C_3N_4 composes of tri-s-triazine and triazine units in 6-membered rings with sp^2-hybridized C and N atoms, which form an aromatic p-conjugated system. The unique stable structure of g-C_3N_4 makes it durable under severely acidic and alkaline conditions (Wang, Maiyalagan et al. 2012, Martin, Reardon et al. 2014).

In addition, The nonporous nature of g-C_3N_4 accompanied by an extremely low specific surface area and the stacking of thick g-C_3N_4 layered structures hinders its application in various fields (Martin, Reardon et al. 2014, Ouyang, Xu et al. 2022). Graphene-like carbon nitride nanosheets (CN-NS) with 2D morphology and large specific surface area has shown a potential performance in photo-catalysis, energy storage and bio-sensing (Wang, Blechert et al. 2012, Liu, Liu et al. 2015, Ong, Tan et al. 2016, Truong, Bae et al. 2021). Therefore, the unique characteristics of g-C_3N_4 also make it a desirable membranes for advanced separation (Wang, Gao et al. 2020).

Another challenge in the preparation of nanostructure-based filters is the adhesion and stability of nanoparticles to the substrate in water-oil separation cycles, which is also a significant issue in this study. The adhesion of thin nanoparticle coatings to the substrate is performed using a combination of modified particles and modified substrates (Ong, Tan et al. 2016) or with the aid of crosslinking agents such as silane groups, polymeric binders and so on (Yoon 2007, Basnar, Litschauer et al. 2012, da Silva, Lucas et al. 2022). Thermoplastic polyurethane (TPU) is commonly used as adhesive to join different materials in automotive and general use adhesives industries (Oertel 1993, Tien and Wei 2001). Therefore, TPU as a binder to increase the adhesion of nanoparticles to the substrate will be investigate in this work.

Because of the previously mentioned advantages of g-C_3N_4-NS and TPU, they might be the favorable material for coating on SSM to render the surface with specific wetting and durability properties. In this study, for the first time, g-C_3N_4-NS is used to modify the surface in order to separate water and oil. In this work, the surface wettability, surface energy and oil-water separation ability of g-C_3N_4/TPU coated SSM

was assessed. Ultimately, facile and scalable synthesis approach, commercially available chemicals of TPU and melamine as a precursor of g-C_3N_4, the g-C_3N_4-NS coated mesh has a great ability for large-scale application for oil-water separation.

Material And Methods

3.1 Chemicals

Stainless steel mesh (SSM) (#316l, opening diameter of 5 µm) with the surface area of 2 cm× 2 cm, Thermoplastic polyurethane (TPU), H_2SO_4 (98.0%), $KMnO_4$, HCl (36.5%), HNO_3 (78.0%) and melamine.

3.2 Preparation of g-C_3N_4 nanosheets

The bulk-g-C_3N_4 (b-CN) was prepared by thermal condensation method (Wang, Blechert et al. 2012). Synthesis of Functionalized g-C_3N_4 nanosheets (CN-NS) was performed using the improved Hummer's method (Hummers Jr and Offeman 1958). Briefly, 5.00 g of b-CN powder was suspended in 150 mL of sulfuric acid under continuous strirring at 333.2 K for 60 min. Then, 7 g of potassium permanganate was moderately added into the mixture while it was placed in an ice bath the solution. Mixture was heated from and stirred at 303.2 K for 60 min. Then, 1500mL deionized water was slowly poured into the mixture within 50 min. Finally, 5% hydrogen peroxide solution was dropped into the suspension to turn its color to milky. The precipitated CN-NS was washed by HCl solution (2%) several times, followed by washing with water and drying in vacuum oven at 303.15 K overnight.

3.3 Coating procedure

Stainless steel mesh was used as substrates in this study. for the preparation of coating materials, TPU (4 wt.%) as a binder was dissolved into DMF, and then CN-NS was added into the DMF solution and ultrasonicated for 3h under 100 W power to obtain CN-NS dispersions in DMF with different mass ratios of CN-NS and TPU (ratio of CN/TPU of 9:1, 8:2, 7:3, 6:4, 5:5, 4:6, 3:2, 2:1 and 1:0 which characterized by A1, A2, A3, A4, A5, A6, A7, A8, A9 and A10, respectively). The prepared solution was coated on the stainless steel mesh substrates using dip-coater with the speed of 3 cm/min. Then, the samples were dried at ambient temperature to let the solvent evaporate completely. The coating procedure was repeated twice again. In this way, The CN-TPU composite film on stainless steel mesh was prepared and used for further testing. Fig. 1 shows a schematic diagram of the fabrication process of CN-TPU composite film.

3.4 Emulsion preparation

Decalin (CAS Ref.-No. 493-01-6, surface tension of 31.5 mN/m) as an alternative model for crude oil (20 mL), which mixed with 2 wt.% of SPAN80 (HLB=4.3) as an emulsifier, and deionized water (20 mL), which was colored with blue dye, were mixed and treated for 3h under stirring rate of 2500rpm to form a water/oil emulsion.

The as-prepared filter was fixed between two glass tubes with diameter of 25 mm. The water/oil emulsion was poured onto the as-prepared mesh. The separation was achieved by the driving force of gravity.

3.5 Characterization

Fourier transform infrared (FTIR, Brucker Tensor27 model) spectroscopy and X-ray powder diffraction (XRD, Inel EQUINOX3000 model) analyses performed to identify functional groups and crystalline structure of b-CN and CN-NS. The surface morphology of CN-coated stainless steel mesh was observed using field emission scanning electron microscopy (FESEM, model MIRA3TESCAN-XMU) equipped with energy dispersive spectroscopy (EDS) to obtain the elemental compositions of the surface of CN-coated stainless steel mesh. SEM images were also obtained with a field emission scanning electron microscope to examine the surface morphology.

Atomic force microscope (AFM, BRUKER, model ICON) in direct contact mode was used to evaluate topographic studies such as roughness of the filter surface. Carbon, nitrogen and hydrogen contents of resultant material, the elemental analyses (CHN analysis, Costech ECS 4010) was carried out. Oil and water contact angle (OCA and WCA) and underwater oil contact angles as the wetting properties of the prepared filter was measured using a video optical contact angle system at ambient temperature. For this purpose, 5μL water droplet was dropped onto the coated substrate and microscopic images of these droplets were analyzed using ImageJ (National Institutes of Health, USA) by three times. Size distribution of dispersed phase in emulsion was measured using dynamic light scattering (DLS) (Cordouan Tech, model VASCO2). The separation efficiency of the prepared filter was calculated using equation (1) (Yang, Yin et al. 2015):

$$R(\%) = (1 - \frac{C_p}{C_0}) \times 100 \quad (1)$$

Where C_0 and C_p are the water or oil content of permeate and retentate.

Results And Discussion

The mechanism of the Hummer's method for the fabrication of exfoliated CN-NS is explained as follow: b-CN is protonated by H_2SO_4 in the beginning of the oxidization process. Then, the edge of the carbon nitride layers is oxidized by $KMnO_4$.

Powder X-ray Diffraction (XRD) measurements of b-CN and CN-NS (exfoliated g-C_3N_4 using Hummer's method) was used to study changes of crystalline structures in the exfoliation process (Fig. 2a). The diffraction peak of b-CN at about 2□=13.1° can be seen in both b-CN and CN-NS. The corresponding angle is indexed as the (100) plane of b-CN caused by the intra-planar structural packing. The strong peak at 2□=27.8179° (d-spacing = 0.3207 nm) is indexed as (002) plane arising from the inter-layer diffraction in graphite-like carbon nitride structures (Niu, Zhang et al. 2012). The peak of Hummer's g-C_3N_4 had moved to the higher angles in comparison with the peaks of b-CN. The diffraction peak (002) of the product is quite in accordance with the diffraction peak (002) and it had move to higher angle of 2□=28.2422° (d-

spacing=0.3944 nm) in Hummer's g-C_3N_4, which causes increasing in the interlayer distance based on Bragg's law. Distance between g-C_3N_4 sheets increased by 0.7$\mathring{A}$ after Hammer's oxidation method. Thus, oxidization exfoliation process showed the desire performance in the protonation process and creates the positive charges on each single layer of graphene-like carbon nitride, which indicates that the spacing enlargement of (002) plane were aroused by the protonation. Moreover, the partly intercalation performance of H_2SO_4 could induce the active site in the subsequent oxidization exfoliation process (Chen, Li et al. 2015). Thus Hummer's method enables nanoparticles to form a good structure and film in the polymer structure or in combination with polymer binders such as TPU, which we will examine this. The crystal size of g-C_3N_4, calculated from the Scherrer equation that relates the crystallite size to the broadening of a peak in a diffraction pattern, decreased from 16.9 to 8.6 nm with Hummer's oxidation method.

The surface wettability for water and/or oil influences by the physical morphology and surface chemistry. Thus, to investigate the surface chemistry and morphology surface chemistry of the modified meshes, FESEM, FTIR, and AFM measurements were conducted. FT-IR was employed to get more insight of the functional groups in CN_NS (Fig. 2b). As shown in Fig. 2b, the characteristic absorption peaks of the tri-s-triazine ring and CN heterocycles are between 1200 and 1600 cm^{-1}. Peak at 801 cm^{-1} indicates the similar covalent bonds between carbon atoms and nitride atoms. The oxidation reaction in Hummer's method is confirmed with the more intense peak at 1071 cm-1 attributed to C=O stretching vibrations compared to that at bulk g-C_3N_4. Adsorption peak at 1678 cm-1 arising from carboxyl and carbonyl are stronger in the spectrum of CN_NS compared with b-CN. The broad peak arouses at around 3100 and 3600 cm^{-1} in the spectrum of CN_NS assigns the NH moieties, as well as to the adsorbed hydroxyl groups of H_2O.

To investigate the nitrogen content of resultant b-CN and CN-NS, the elemental analyses of carbon, nitrogen and hydrogen are shown in Table 1. The C/N ratio increases from 0.634 for the bulk g-C_3N_4 to 0.701 for the CN-NS one, which is due to nitrogen loss. In the exfoliation process, oxygen atoms substitutes by oxidized nitrogen atoms and consequently results in nitrogen loss in CN-NS sample. The C/N ratio for both b-CN and CN-NS was lower than 0.75 for the ideal g-C_3N_4 crystal which justified with reduction of the hydrogen contents in polymerization time. The residual hydrogen atoms, in the incomplete polycondensation process, formed 2C-NH and C-NH2 bonds with bonding to the edges of g-C_3N_4 sheet.

Additionally, Brunauer-Emmett-Teller (BET) method was carried out to measure the specific surface area (SSA), pore volume and pore size of the as-prepared bulk g-C_3N_4 and Hummer's g-C_3N_4 (Table 1). Fig. 3 (a-c) represents the nitrogen adsorption-desorption isotherms and pore size distribution of bulk and Hummer's g-C_3N_4. Pore radius and SSA were determined by the BJH method (Fig. c,d). It can be clearly seen that both samples showed a typical type III isotherm with a H3 hysteresis loop according to the IUPAC classification. Using Hummer's exfoliation process, the SSA and pore volume of g-C_3N_4 increased

from 12.023 $m^2.g^{-1}$ and 0.06 $cm^3.g^{-1}$ to 114.4 $m^2.g^{-1}$ and 0.74 $cm^3.g^{-1}$, respectively. The pore size of the g-C_3N_4 decreased to 15.218 nm after Hummer's exfoliation process. These results strongly confirm that in Hummer's method, bulk-g-C3N4 has been successfully exfoliated into nanosheets and their porosity has increased.

Table 1: CHN analysis of g-C_3N_4 bulk and modified g-C_3N_4 with Hummer's method

Sample name	composition				porosity		
	%C	%N	%H	C/N ratio	SBET b/m2 g_1	Pore volumeb/cm3 g_1	Pore sizeb/nm
Bulk g-C3N4	26.95	49.6	3.38	0.634	12.023	0.0675	22.457
Hummer's g-C3N4	28.96	48.2	3.35	0.701	114.4	0.7362	15.218

Large amount of oxygenous functional groups has given special importance to CN-NS for their application. For instant, CN-NS with oxygenous functional groups can apply as a reactant for graft copolymerization. This issue is especially important in this study because it has been tried to coat carbon nitrides on a stainless steel mesh surface with the aid of a polymer binder to make strong bonding of the film to the substrate.

In order to investigate the uniform film formation of CN-NS and TPU binder on stainless steel mesh, the images taken from FESEM are shown in the Fig. 4. It is obvious from FESEM images (Fig. 4a-c) that there is no area on the wires of mesh that is not covered with the coating material. This confirms film formation and the successful assembly of CN-TPU on the mesh wires. In other words, there is no significant re-stacking of CN-NS in the composite and CN-NS is well dispersed in the polymer matrix. As can be observed, CN-NS creates the nano-micrometer scale roughness and formed many cavities because of its low surface energy, which is discussed later. The structure of the micro-nanometer roughness operates in such a way that could result in trapping air in oil and water droplets and consequently causes an increment in the contact angle of the coating layer with the solid surface (Facio and Mosquera 2013). Moreover, flower-like micrometer-scale aggregates from can be discovered on the surface of coated mesh (Fig. 4a-c). There are also smaller carbon nitride nanoparticles with an average diameter of 35 nm on the surface of coated mesh.

EDS spectra in Fig. 4d, which illustrates the chemical composition of CN-TPU film coated on the surface of substrate, showed that the wires are enriched with carbon, nitrogen and oxygen on the surface of the

mesh and confirms the successful synthesis of CN-TPU composite. The homogenous distribution of these elements on the mesh wires also confirms by the elemental mapping results, shown in Fig. 4d.

4.1 Contact angle and interfacial tension measurements

Hydrophilicity and oleophilicity, indicating the tendency of the surface to water or oil, are decisive factors for a surface to apply for oil-water separation. These wettability factors were determined by water contact angle (WCA) in air and oil contact angle (OCA). Thus, at first step we examined the effect of g-C_3N_4 and TPU concentration on surface wettability (A1-A10, Table 2). Decalin as a sample oil was used to measure OCA. Unmodified bulk carbon nitride (bulk g-C_3N_4) showed hydrophobic behavior with a WCA and underwater OCA of 98.6° and 135.55°, respectively, which by post treatment using Hammer's method, its wettability properties changed significantly towards hydrophilicity and superhydrophilivity from sample 1 to 10.

The results indicates that the WCA increases with increasing the concentration of g-C_3N_4-NS, but the OCA remained constant at 0° for all samples. As indicated in Fig. 5, WCA for filter coated with TPU (A10) was 88° and it will be gradually decrease with the addition of CN-NS. Hydrophilic TPU was used to make the coating more adhesive. However, all filters, including filter A1, show superoleophilic behavior in air with OCA of 0°.

Although hydrophilic behavior appeared for TPU coated mesh, WCA has been increased with addition of CN-NS. Increasing the concentration of CN nanoparticles in coating composition of A8 to A9 efficiently decreased the WCA from 32° to 0°. Indeed with increasing the CN-NS composite on coating materials, it can be seen that hydrophilicity gradually maximized for A1 sample with the CN/TPU ratio of 9:1, which confirms the superhydrophilic behavior. For A1 filter, underwater OCA was examined and results show that A1 has underwater oleophobic behavior with OCA of 155° (Fig. 6). Therefore, A1 is a superhydrophilic/underwater superoleophobic, while the other filters are superoleophilic/hydrophilic in air.

Table 1
The composition of for different synthesized coatings on SSM

ID	CN/TPU wt.% ratio	WCA (°)	Underwater OCA (°)
Bulk g-C_3N_4	9/1	98.6	135.55
A1	9/1	0	155
A2	8/2	32	100
A3	7/3	55	
A4	6/4	77	-
A5	5/5	78	95
A6	4/6	80	-
A7	3/7	85	75
A8	2/8	87	-
A9	1/9	87	-
A10	0/1	88	-

Phase separation occurs in coating composition and carbon nitride CN-NS comes to the surface of the filter and plays a role in controlling the surface wettability. This improvement in properties caused by the formation of hydrogen bonds between the soft segments of the TPU and the hydroxyl groups on the CN-NS surface (Nunes, Fonseca et al. 2000, Nunes, Pereira et al. 2001). Carbon nitride nanoparticles are inherently hydrophilic with functional groups on their edge, thus increasing the hydrophilic properties of the surface. In addition, with the arrival of nanoparticles on the filter surface, in turn, the surface roughness increases according to the Cassie–Baxter state and efficiently causes more hydrophilic surface (Facio and Mosquera 2013).

AFM analysis was carried out to deals with the effect of CN nanoparticles on the surface roughness. Fig. 7 indicates the AFM micrographs and the surface topography of the CN-NS coated-mesh of A5 and A1. AFM results reveal that the Root Mean Square (RMS) roughness (Rq) is 0.14 μm and 0.154 μm for A5 and A1 (Fig. 7a,b), respectively. Therefore, the surface roughness of A1 is higher than of A5. Increasing the surface roughness has led to the conversion of the surface from hydrophilic (A5) to superhydrophilic (A1). Roughness increases the wettability of the hydrophilic CN-NS coated surface. Furthermore, the micrographs of AFM results indicate the micro/nanoscale roughness that is the result of packing the CN-NS together.

There is a good correlation between the wettability and surface energy. Therefore, the interface energy, which composed of non-dispersive or polar component (γ^p) and polar component (γ^d), was calculated for CN-NS/TPU (A1 and A5) by Geometric-mean relation (Wu 1982) as follow:

$$\cos\theta_W = \frac{2\sqrt{\gamma_{SV}^d \gamma_{WV}^d} + 2\sqrt{\gamma_{SV}^p \gamma_{WV}^p}}{\gamma_{WV}^d + \gamma_{WV}^p} - 1 \quad (2)$$

$$\cos\theta_O = 2\sqrt{\frac{\gamma_{SV}^d}{\gamma_{OV}^d}} - 1 \quad (3)$$

Where; γ_{SV}^d and γ_{SV}^p are the dispersive and polar components of surface energy, and θ denotes the contact angle. Two probe liquids of water and decalin was used to calculate these two components. The values of the surface tension of these liquids and their polar and dispersive components are shown in Table 2. The obtained surface energy of A1 (74.07 mJ/m^2) is higher than of water's surface tension (72.8 mJ/m^2), While A5 has the surface energy (37.68 mJ/m^2) close to the surface tension of decalin (31.5 mJ/m^2). This implies that A1 and A5 have more affinity to become wet with water and decalin, respectively.

Table 2
Data of surface tension and its components of the probe liquids used in this work

component	γ^p(mJ/m^2)	γ^d (mJ/m^2)	γ (mJ/m^2)
Water	51.0	21.8	72.8
Decalin	0.0	31.5	31.5
A1	42.57	31.5	74.07
A5	6.186	31.5	37.68

Therefore, filters A1 (with 9:1 ratio of CN:TPU, underwater OCA=155° and WCA=0°) and A5 (with 5:5 ratio of CN:TPU, OCA=0° and WCA=78°), were mounted in the separation setup ,shown in Fig. 8, to investigate their ability to separate the water and oil emulsion. As can be seen in the figure, after pouring the emulsion, decalin passed through filter A5, which had superoleophilic behavior, and effectively separated from emulsion with the efficiency of 99%. Because A5 filter exhibits oil affinity rather than water, it demonstrates the water repellency. Decalin has turned yellow after passing through coated mesh due to presence of oil-soluble Span-80 emulsifier (Fig. 8a).

Pre-wetted filter of A1 with superhydrophilic and underwater superoleophobic behavior separated water from the prepared water-in-oil emulsion with the efficiency of 79% (Fig. 8b). Although this filter has passed oil along with water with some extent, its good performance in separating water is due to its pre-wetting, which allows it to show its wettability behavior of underwater superoleophobicity. Indeed, high degree of surface roughness leads to trap water and subsequently the transition of Wenzel to Cassie

state of underwater oil droplet (Yong, Chen et al. 2017). It should be noted that the emulsion separation is partly due to the small pore size of the stainless steel mesh, which is about 5 μm.

Permeate flux of A5 for separation of decalin from water-in-decalin emulsion is about 50 $L.m^{-2}.h^{-1}$, while this value is lower for separation of water using pre-wetted A1 filter and it measured as 45 $L.m^{-2}.h^{-1}$. This is because the flux of the water-rich permeate in separation of emulsified water-oil mixture is limited by the sedimentation velocity of water droplets, which are the dispersed phase. Droplet size before and after separation was measured using DLS measurement and shown in Fig. 8(c,d). The droplet size of the water-in-decalin emulsion feed is distributed from 100 nm to about 1.2 μm, while the size distribution of water droplets has been increased to 500 nm to 10 μm in permeate, which showed the coalescence of water droplets once contacting with the coatings of the mesh. Therefore, coalescence separation is dominated in case the size of the emulsion droplets is smaller than the average diameter of pores of TPU/g-C_3N_4 coated-mesh (Dang, Liu et al. 2016). This mechanism happens by the coalescence of droplets when contacting with the coatings of the mesh as shown in Fig. 8e. It is noted that the size distribution of dispersed phase in permeate justified that water-in-decalin emulsion could not be completely demulsified.

Figure 9a,b shows the solely gravity-driven separation of free decalin and water using A1 and A5 g-C_3N_4/TPU filters. As can be seen in Fig. 9a, decalin was flowed through A5 filter while water was repelled (supplementary movie 1). Pre-wetted A1 filter did the opposite, passing water and rejecting decalin (Fig. 9b) (supplementary movie 2). Permeate flux for separating free water-oil mixture (50%) was about 6114 $L.m^{-2}.h^{-1}$ (efficiency of ~99.99%) for both A1 and A5 coated filters.

Generally, the separation mechanism of two filters with different wettability properties is justified as follow: 1) hierarchical nano-micrometer scale roughness structures formed by the CN-NS on the surface; 2) hydrophilic features and surface energy reduction using the high amount of hydrophilic CN-NS and 3) SSM with a smaller pore size of about 5 μm. it seems that the presence of more polar groups (OH and COOH), especially for A1 filter with higher concentration of CN-NS, combined with the special morphological structures observed by FESEM and AFM are responsible for the different surface wettability.

That being said, both A1 and A5 filters have a good ability to separate oil and water emulsions. It should be noted that since the filters are made of inexpensive carbon nitride materials and TPU polymeric binder, as well as do not require complex preparation methods, they can be a good alternative to other filters for commercialization.

Conclusion

In conclusion, g-C_3N_4/TPU-coated stainless steel meshes were fabricated via dip-coating method to investigate the capability of graphitic carbon nitride (g-C_3N_4) in oil-water separation. The uniform coating of g-C_3N_4/TPU endowed the mesh with superhydrophilicity/underwater superoleophobicity and superoleophilicity at the g-C_3N_4:TPU ratio of 9:1 and 1:1, respectively. The first filter with superhydrophilic/underwater superoleophobic behavior permeated water from emulsified wate-in-oil mixture with 79% efficiency. The later one with superoleophilic behavior could selectively separate oil from emulsion driven by gravity with high water rejection (~99.00%). Both filters were able to separate free water and oil mixtures with flux and efficiency of 6114 $L.m^{-2}.h^{-1}$ and ~99.99%, respectively. Surface energy of both filters was calculated and implied that A1 with superhydrophilic/underwater superoleophobic behavior and A5 with superoleophilic behavior have more affinity to become wet with water and decalin, respectively. In addition, surface roughness, functional groups on the surface and stainless steel mesh with a smaller average pore size of about 5μm are responsible for efficient separation of water-in-oil emulsion.

Thus, we envision that this g-C_3N_4/TPU coated mesh has potentials for applications in the industrial scale for oil-water separation. Because this technology employs commercially available polymeric binder, a very simple and fast coating process, as well as facile preparation process of g-C_3N_4 from available and inexpensive precursor, it has great potential for large-scale applications for oil-water separation.

Declarations

Acknowledgements

We gratefully thank Iran national science foundation (INSF) (NO.99018352) for the financial support. We are also thanks the Research Institute of Petroleum Industry (RIPI) and the Department of Chemical Engineering, Amirkabir University of technology (Tehran Polytechnic), Tehran, Iran.

Ethical Approval

Not applicable.

Consent to Participate

Not applicable.

Consent to Publish

Not applicable.

Authors Contributions

Sonia Mir as PhD students carried out the experiments of this research as her PhD thesis. Proff. Rashidi and Dr.Naderifar as supervisor help to get results. Dr. Alaei as advisor help to draft the manuscript. The authors read and approved the final manuscript.

Funding

This research in funded by Iran national science foundation (INSF) (NO.99018352) for the financial support. We are also thanks the Research Institute of Petroleum Industry (RIPI) and the Department of Chemical Engineering, Amirkabir University of technology (Tehran Polytechnic), Tehran, Iran.

Competing Interests

The authors declare that they have no competing interest.

Availability of data and materials

All relevant data and materials are presented within this context.

References

1. Agano, C. B., A. G. C. Villanueva, A. P. S. Cristobal, R. G. B. Madera, A. D. S. Montallana and M. R. Vasquez Jr (2021). "Fabrication of superhydrophilic and underwater superoleophobic CuxO/TiO2 mesh for oil–water separation." Results in Physics 25: 104257.
2. Basnar, B., M. Litschauer, G. Strasser and M.-A. Neouze (2012). "Analyzing imidazolium bridging in nanoparticle networks covalently linked to silicon substrates." The Journal of Physical Chemistry C 116(16): 9343-9350.
3. Chen, J., Y. Li, L. Huang, C. Li and G. Shi (2015). "High-yield preparation of graphene oxide from small graphite flakes via an improved Hummers method with a simple purification process." Carbon 81: 826-834.
4. da Silva, Í. G., E. F. Lucas and R. Advincula (2022). "Highly efficient Oil/Water and brine Separations: Superhydrophobic hybrid isobornyl methacrylate coatings." Separation and Purification Technology 278: 119365.
5. Dang, Z., L. Liu, Y. Li, Y. Xiang and G. Guo (2016). "In situ and ex situ pH-responsive coatings with switchable wettability for controllable oil/water separation." ACS applied materials & interfaces 8(45): 31281-31288.
6. Du, X., G. Zou, Z. Wang and X. Wang (2015). "A scalable chemical route to soluble acidified graphitic carbon nitride: an ideal precursor for isolated ultrathin gC 3 N 4 nanosheets." Nanoscale 7(19): 8701-8706.
7. Facio, D. S. and M. J. Mosquera (2013). "Simple strategy for producing superhydrophobic nanocomposite coatings in situ on a building substrate." ACS Applied Materials & Interfaces 5(15): 7517-7526.

8. Fang, J., H. Fan, M. Li and C. Long (2015). "Nitrogen self-doped graphitic carbon nitride as efficient visible light photocatalyst for hydrogen evolution." Journal of Materials Chemistry A 3(26): 13819-13826.
9. Hummers Jr, W. S. and R. E. Offeman (1958). "Preparation of graphitic oxide." Journal of the american chemical society 80(6): 1339-1339.
10. Li, G., Z. Lian, W. Wang, D. Zhang and H. Li (2016). "Nanotube-confinement induced size-controllable g-C3N4 quantum dots modified single-crystalline TiO2 nanotube arrays for stable synergetic photoelectrocatalysis." Nano Energy 19: 446-454.
11. Lin, Y., M. S. Salem, L. Zhang, Q. Shen, A. H. El-shazly, N. Nady and H. Matsuyama (2020). "Development of Janus membrane with controllable asymmetric wettability for highly-efficient oil/water emulsions separation." Journal of Membrane Science 606: 118141.
12. Liu, J., W. Li, L. Duan, X. Li, L. Ji, Z. Geng, K. Huang, L. Lu, L. Zhou and Z. Liu (2015). "A graphene-like oxygenated carbon nitride material for improved cycle-life lithium/sulfur batteries." Nano letters 15(8): 5137-5142.
13. Liu, J., Y. Liu, N. Liu, Y. Han, X. Zhang, H. Huang, Y. Lifshitz, S.-T. Lee, J. Zhong and Z. Kang (2015). "Metal-free efficient photocatalyst for stable visible water splitting via a two-electron pathway." Science 347(6225): 970-974.
14. Martin, D. J., P. J. T. Reardon, S. J. Moniz and J. Tang (2014). "Visible light-driven pure water splitting by a nature-inspired organic semiconductor-based system." Journal of the American Chemical Society 136(36): 12568-12571.
15. Niu, P., L. Zhang, G. Liu and H. M. Cheng (2012). "Graphene-like carbon nitride nanosheets for improved photocatalytic activities." Advanced Functional Materials 22(22): 4763-4770.
16. Nunes, R., J. Fonseca and M. Pereira (2000). "Polymer–filler interactions and mechanical properties of a polyurethane elastomer." Polymer testing 19(1): 93-103.
17. Nunes, R., R. Pereira, J. Fonseca and M. Pereira (2001). "X-ray studies on compositions of polyurethane and silica." Polymer Testing 20(6): 707-712.
18. Oertel, G. (1993). "Polyurethane Handbook 2nd edn (Munich: Hanser)."
19. Ong, W.-J., L.-L. Tan, Y. H. Ng, S.-T. Yong and S.-P. Chai (2016). "Graphitic carbon nitride (g-C3N4)-based photocatalysts for artificial photosynthesis and environmental remediation: are we a step closer to achieving sustainability?" Chemical reviews 116(12): 7159-7329.
20. Ouyang, K., B. Xu, C. Yang, H. Wang, P. Zhan and S. Xie (2022). "Synthesis of a novel Z-scheme Ag/WO3/g-C3N4 nanophotocatalyst for degradation of oxytetracycline hydrochloride under visible light." Materials Science in Semiconductor Processing 137: 106168.
21. Song, J., S. Huang, Y. Lu, X. Bu, J. E. Mates, A. Ghosh, R. Ganguly, C. J. Carmalt, I. P. Parkin and W. Xu (2014). "Self-driven one-step oil removal from oil spill on water via selective-wettability steel mesh." ACS applied materials & interfaces 6(22): 19858-19865.
22. Su, M., Y. Liu, Y. Zhang, Z. Wang, Y. Li and P. He (2018). "Robust and underwater superoleophobic coating with excellent corrosion and biofouling resistance in harsh environments." Applied Surface

Science 436: 152-161.

23. Sun, B., F. Zhang, M. Gao, S. Zhao, J. Wang, W. Zhang, Z. Wang and J. Wang (2020). "Superhydrophilic Stainless Steel Mesh for Oil–Water Separation with Long-Term Durability, Impressive Corrosion Resistance, and Abrasion Resistance." Advanced Engineering Materials 22(8): 2000262.
24. Tian, D., X. Zhang, Y. Tian, Y. Wu, X. Wang, J. Zhai and L. Jiang (2012). "Photo-induced water–oil separation based on switchable superhydrophobicity–superhydrophilicity and underwater superoleophobicity of the aligned ZnO nanorod array-coated mesh films." Journal of Materials Chemistry 22(37): 19652-19657.
25. Tian, D., X. Zhang, X. Wang, J. Zhai and L. Jiang (2011). "Micro/nanoscale hierarchical structured ZnO mesh film for separation of water and oil." Physical Chemistry Chemical Physics 13(32): 14606-14610.
26. Tien, Y. and K.-H. Wei (2001). "Hydrogen bonding and mechanical properties in segmented montmorillonite/polyurethane nanocomposites of different hard segment ratios." Polymer 42(7): 3213-3221.
27. Truong, H. B., S. Bae, J. Cho and J. Hur (2021). "Advances in application of g–C3N4–based materials for treatment of polluted water and wastewater via activation of oxidants and photoelectrocatalysis: A comprehensive review." Chemosphere: 131737.
28. Wang, H., T. Maiyalagan and X. J. d. o. c. Wang (2012). "Review on Recent Progress in Nitrogen-doped graphene: synthesis, characterization, and its potential applications. ACS Catal. 2, 781–794 (2012)." 652.
29. Wang, X., S. Blechert and M. Antonietti (2012). "Polymeric graphitic carbon nitride for heterogeneous photocatalysis." Acs Catalysis 2(8): 1596-1606.
30. Wang, X., S. Blechert and M. J. A. C. Antonietti (2012). "Polymeric graphitic carbon nitride for heterogeneous photocatalysis." 2(8): 1596-1606.
31. Wang, Y., B. Gao, Q. Yue and Z. Wang (2020). "Graphitic carbon nitride (gC 3 N 4)-based membranes for advanced separation." Journal of Materials Chemistry A 8(37): 19133-19155.
32. Wang, Y., B. Wang, Q. Wang, J. Di, S. Miao and J. Yu (2018). "Amino-functionalized porous nanofibrous membranes for simultaneous removal of oil and heavy-metal ions from wastewater." ACS applied materials & interfaces 11(1): 1672-1679.
33. Wu, S. (1982). Polymer interface and adhesion: Souheng Wu, M. Dekker: New York.
34. Xie, J., J. Zhang, S. Li, F. Grote, X. Zhang, H. Zhang, R. Wang, Y. Lei, B. Pan and Y. Xie (2013). "Controllable disorder engineering in oxygen-incorporated MoS2 ultrathin nanosheets for efficient hydrogen evolution." Journal of the American Chemical Society 135(47): 17881-17888.
35. Yang, H., P. Pi, Z.-Q. Cai, X. Wen, X. Wang, J. Cheng and Z.-r. Yang (2010). "Facile preparation of super-hydrophobic and super-oleophilic silica film on stainless steel mesh via sol–gel process." Applied Surface Science 256(13): 4095-4102.

36. Yang, J., L. Yin, H. Tang, H. Song, X. Gao, K. Liang and C. Li (2015). "Polyelectrolyte-fluorosurfactant complex-based meshes with superhydrophilicity and superoleophobicity for oil/water separation." Chemical Engineering Journal 268: 245-250.
37. Yong, J., F. Chen, Q. Yang, J. Huo and X. Hou (2017). "Superoleophobic surfaces." Chemical Society Reviews 46(14): 4168-4217.
38. Yoon, K. B. (2007). "Organization of zeolite microcrystals for production of functional materials." Accounts of chemical research 40(1): 29-40.
39. Yu, Y., H. Chen, Y. Liu, V. Craig, L. H. Li and Y. Chen (2014). "Superhydrophobic and superoleophilic boron nitride nanotube-coated stainless steel meshes for oil and water separation." Advanced Materials Interfaces 1(1): 1300002.
40. Zhang, L., R. Wang, J. Wang, L. Wu and X. Zhang (2019). "Mechanically robust nanocomposites from screen-printable polymer/graphene nanosheet pastes." Nanoscale 11(5): 2343-2354.
41. Zhu, X., A. Dudchenko, X. Gu and D. Jassby (2017). "Surfactant-stabilized oil separation from water using ultrafiltration and nanofiltration." Journal of membrane science 529: 159-169.

Figures

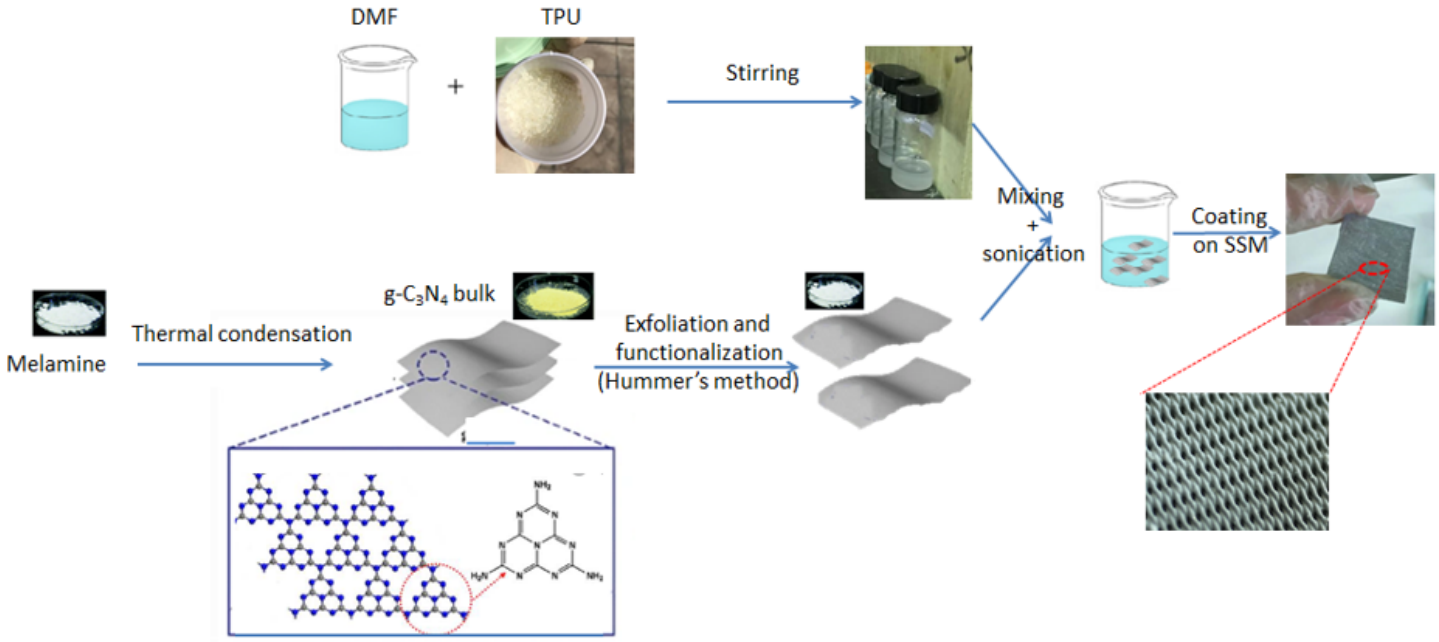

Figure 1

schematic diagram of the preparation process of CN-TPU coated SSM

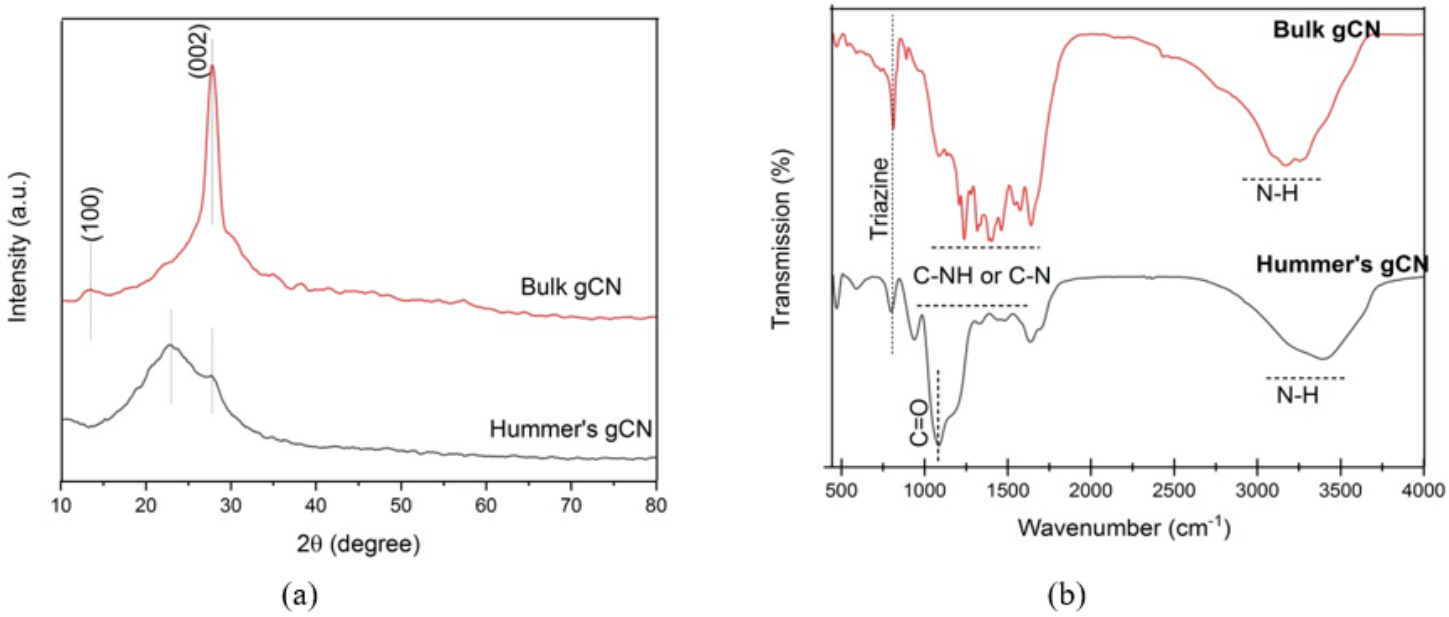

Figure 2

a) XRD patterns of Bulk g-C_3N_4 and b) Hummer's g-C_3N_4 FTIR spectra of Bulk g-C_3N_4 and Hummer's g-C_3N_4

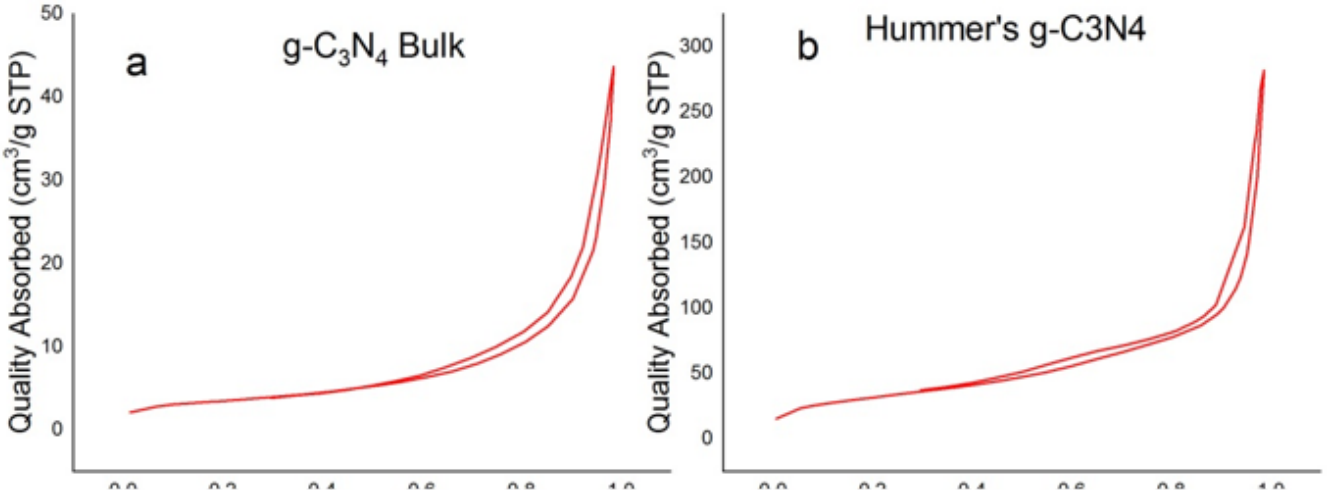

Figure 3

(a) and (c) N_2 adsorption and desorption curves of Bulk g-C_3N_4. (b) and (d) Pore size distribution of Hummer's g-C_3N_4.

Figure 4

Field emission scanning electron microscope (FESEM) images of carbon nitride coated mesh. (a–c) Morphology of the CN-NS/TPU nanoparticle-coated SSM wires (A1) with the scale bar of 100, 20 μm, and 200 nm, respectively; (d) EDS spectra and elemental mapping of C, N, and O on the surface of the CN-NS/TPU coated SSM

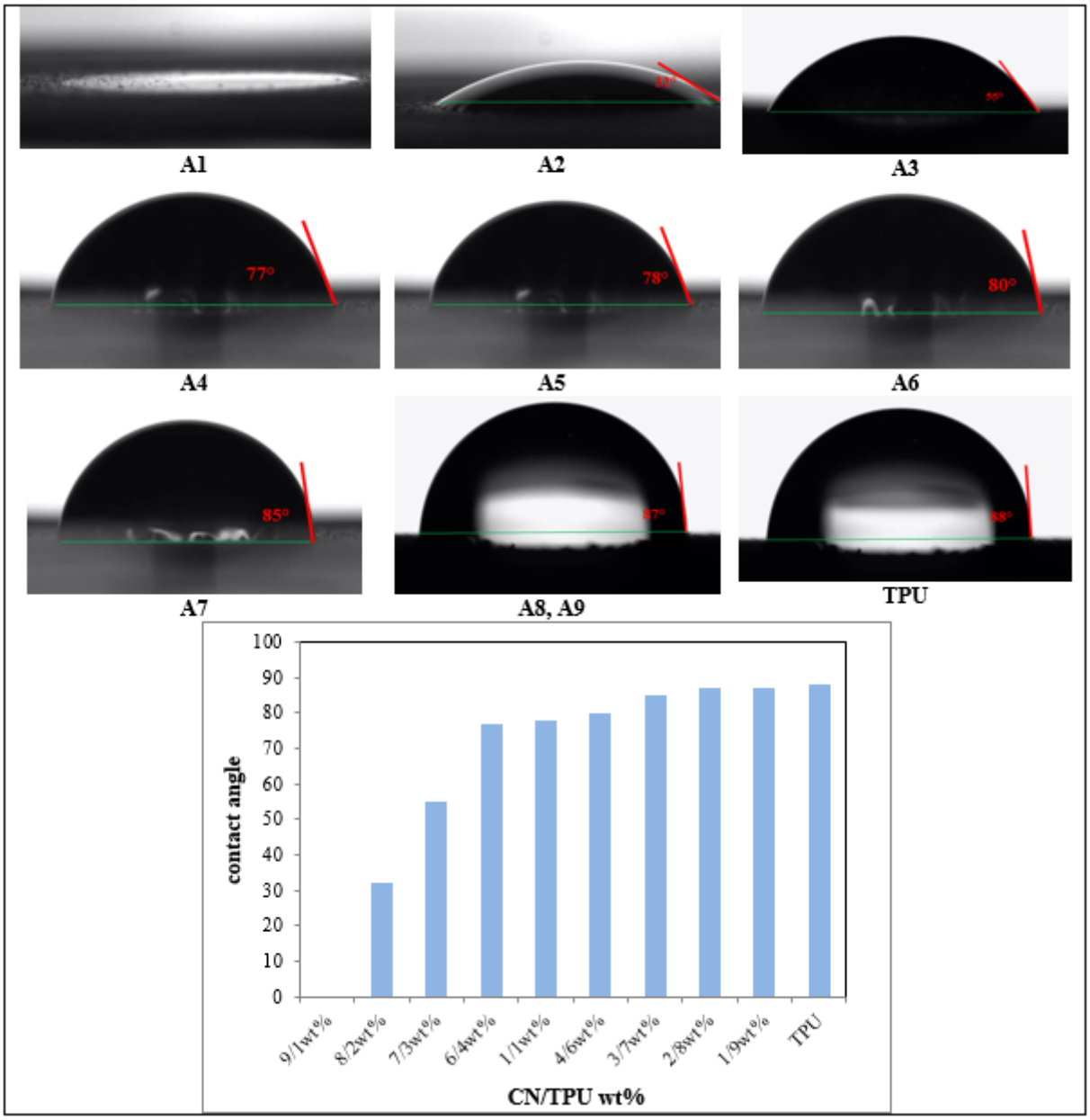

Figure 5

An investigation on the effect of g-C_3N_4 and TPU (A1–A10) concentrations on water contact angles (WCA)

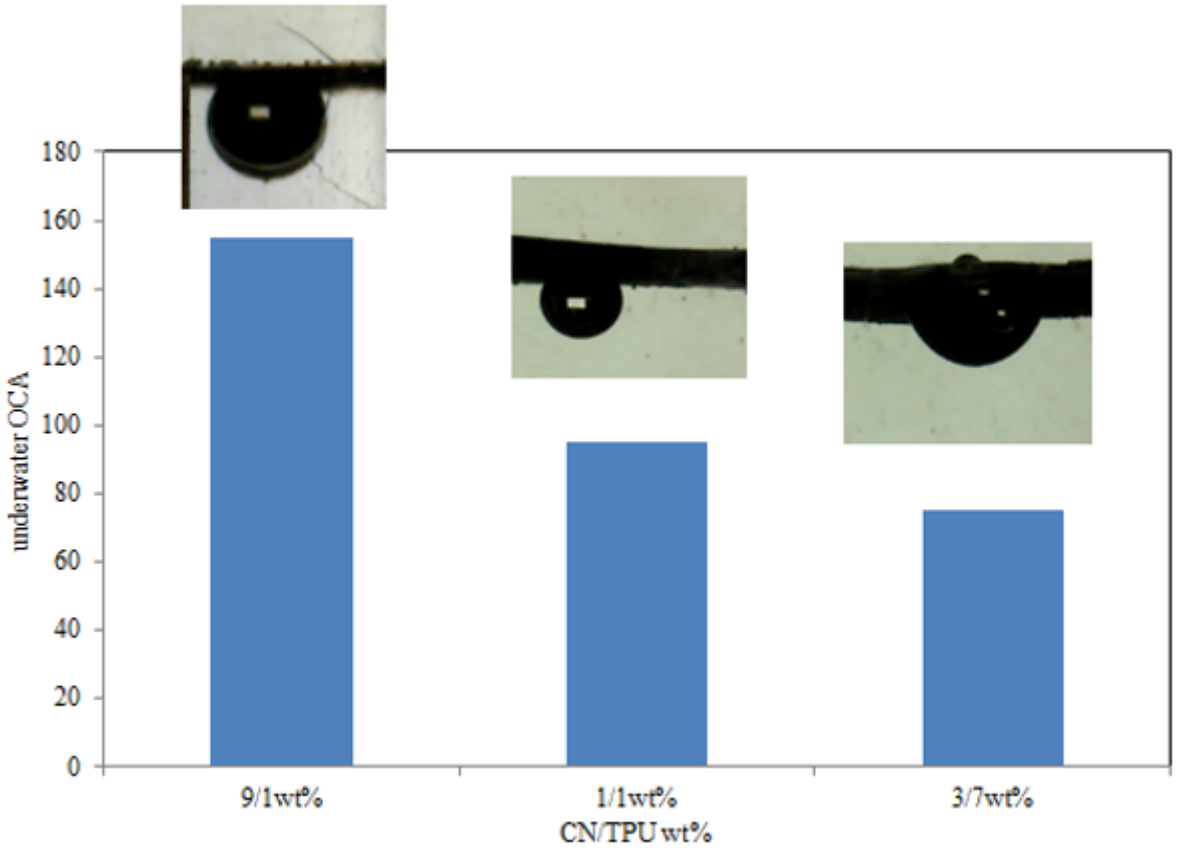

Figure 6

An investigation on the effect of g-C_3N_4 and TPU (A1, A5 and A7) concentrations on underwater oil contact angles

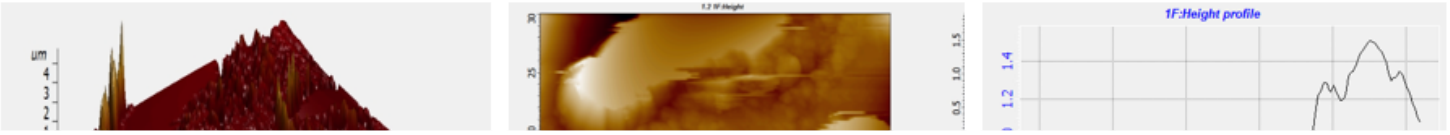

Figure 7

3D and 2D AFM images of the g-C_3N_4 coated mesh surface. a) A5 b) A1

Figure 8

Separation of a water-in-decalin emulsion (50 wt.% of water) by a a) superhydrophilic/underwater superoleophobic coated mesh with CN:TPU ratio of 5:5 (A5). And b) superoleophilic coated mesh with CN:TPU ratio of 9:1 (A1). (c,d) DLS of water-in-decalin emulsion before and after separation by A1 coated mesh, respectively. e) illustration mechanism of coalescing process of demulsified water-oil mixture.

Figure 9

a) **Oil (colourless) passed through the superhydrophilic/underwater superoleophobic coated mesh with CN:TPU ratio of 5:5 (A5) coated mesh, while water (dyed blue) remained on the upper glass tube. b) Water passed through the superoleophilic g-C3N4/TPU coated mesh with CN:TPU ratio of 9:1 (A1) coated mesh, while oil remained on the upper glass tube.**

Supplementary Files

This is a list of supplementary files associated with this preprint. Click to download.

- suppmovie1.mp4
- suppmovie2.mp4